J. Fluid Mech. (1975), *vol.* 69, *part* 3, *pp.* 445–464
Printed in Great Britain

On the role of density jumps in the reflexion and breaking of internal gravity waves

By DONALD P. DELISI AND ISIDORO ORLANSKI
Geophysical Fluid Dynamics Laboratory/NOAA, Princeton University

(Received 11 March 1974)

A laboratory experiment is presented which examines the role of density jumps in the reflexion and breaking of internal gravity waves. It is found that the measured phase shift of the reflected wave and the measured amplitude of the density jump are in good agreement with linear theory. Local overturning occurs when wave amplitude becomes large, and there appears to be a critical amplitude above which overturning will occur and below which it will not. The overturning seems to be due to local gravitational instability, caused by the horizontal advection of density. Overturning changes the basic flow field in the region of interaction; and it results in smaller-scale motions.

1. Introduction

The generation of turbulence by the overturning of internal gravity waves is an important factor in the microscale dynamics of the atmosphere and the oceans. In the atmosphere, the overturning of internal gravity waves and the resulting turbulence are thought to be a primary cause of clear air turbulence and a major source of internal mixing in the atmosphere (see e.g. Pao & Goldberg 1969). In the ocean, the overturning of internal gravity waves is a mechanism for the generation of turbulence in the thermocline. This turbulence enhances vertical mixing in the oceans; and it is a means by which the step structures seen in the oceans can be formed and maintained.

It is commonly thought that most observed overturnings of internal gravity waves are the result of shear (Kelvin–Helmholtz) instabilities, which grow to finite-amplitude billows. As a result, this mechanism has been widely investigated. In the atmosphere, FM/CW radar soundings have been studied by Gossard, Richter & Jensen (1973), and these soundings show many instances of structures that appear to be caused by Kelvin–Helmholtz instabilities. Woods & Wiley (1972) have proposed that the observed layered structure in the ocean is the result of the overturning of finite-amplitude billows, and that the turbulence resulting from the growth and overturning of these billows is the principal mechanism for vertical mixing in the ocean. Experimentally, Kelvin–Helmholtz instabilities, their growth to finite amplitude, and their subsequent overturning have been studied by Thorpe (1968, 1969, 1971, 1973), Scotti & Corcos (1972), Delisi (1972) and Delisi & Corcos (1973). In all of these instances, vertical shear is a primary factor in the growth of the wave and its subsequent overturning.

A different mechanism for the overturning of internal gravity waves was proposed by Orlanski & Bryan (1969). In their model, slowly growing waves would overturn owing to convective instability caused by the horizontal advection of density. For this to occur, the horizontal advection of density must balance the local time rate of change of density. For a single wave, this is true when the horizontal particle velocity equals the horizontal phase velocity. Orlanski (1972) performed a laboratory experiment with a resonant standing wave in a salt-water tank and found that local convective instability preceded turbulence. A nonlinear numerical model confirmed his laboratory experiment. In his analysis, Orlanski found that higher-order wavenumbers were generated in the system naturally, as a result of the nonlinearity of the governing equations. McEwan (1971), in a similar experiment, explained that the higher wavenumbers he observed were the result of free wave modes growing from the noise level and forming resonant triads with the original wave. In a later experiment, McEwan (1973) crossed two beams of internal waves of different amplitude and frequency and explained the resulting regions of intense density gradients, or 'traumata', which preceded turbulence, as the result of nonlinear interactions.

In the atmosphere, the overturning of internal gravity waves is prevalent near the inversion layer; and, in the oceans, the step structure is most clearly visible in and near the thermocline. The aim of the present study is to explore the role of density jumps on the reflexion and breaking of internal gravity waves, to learn more about the overturning process and the resulting turbulence. This experiment generalizes the results of Orlanski's (1972) standing-wave experiment, and considers propagating bands of rays reflecting from a density jump. Although we have used a simplified density structure in the experiment presented here, it is believed that the results can be applied to other, less simplified structures in the atmosphere and the ocean. Thus, the experiment presented in this paper can give some hint as to the role of the inversion layer and the thermocline in the breaking of internal gravity waves.

The following section discusses the experimental equipment used in this study. This is followed in § 3 by a discussion of the linear wave theory and measurements. Section 4 deals with the breaking of internal gravity waves.

2. The experiment

2.1. *Description of the apparatus*

The experiment was performed in a rectangular Plexiglas tank 150 cm long, 89 deep and 28 wide (see figure 1). The tank was filled with salt water before each experiment by a method similar to that of Fortuin (1960) and Orlanski (1972). First, a layer of fresh water several centimetres thick was placed in the tank. Then a constant flow metering pump slowly filled the tank from the bottom with an increasingly more saline solution of salt and water. This solution was obtained by connecting the inlet of the metering pump to a storage tank of fresh water, which was itself connected to a storage tank of brine. The resulting stratification in the wave tank was very nearly linear with height; and the gradient could be adjusted by varying the initial salinity in the salt-water storage tank.

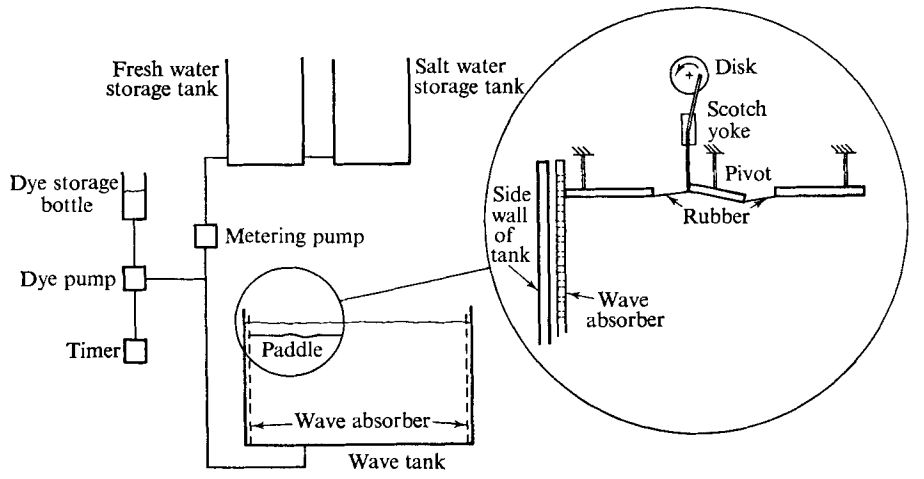

FIGURE 1. Schematic of the experimental apparatus showing the filling mechanism for the wave tank and details of the paddle used as the wave generator.

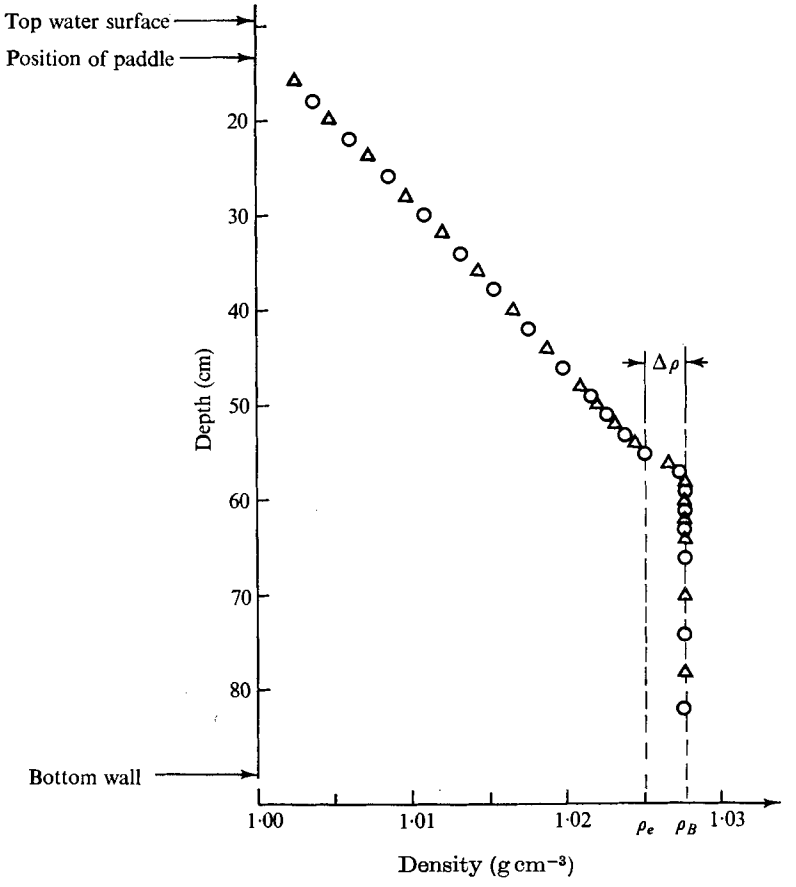

FIGURE 2. A typical density profile as a function of depth measured with a conductivity probe and the traversing mechanism. The positions of the top water surface, paddle and bottom wall of the tank are also marked. ○, downward traverse; △, upward.

A region of constant density fluid was added to the wave tank below the linearly stratified region. To obtain this solution, the remaining fluid in the fresh-water storage tank was discarded, and a solution of the desired salinity was mixed in the salt-water storage tank. This new solution was then allowed to flow into the fresh-water storage tank and into the wave tank. Constant density fluid was added to the tank until the top of the linearly stratified region reached the same level as the wave paddle.

A typical measured density profile is shown in figure 2. The positions of the paddle, top, and bottom surfaces are also shown. The thin, top layer of fresh water, which is not shown on the plot, but which extended from the paddle to the top surface, was added for several reasons. First, it allowed the height of the linearly stratified region from the paddle to the density jump to remain constant across the tank without allowing the paddle to break the water–air surface. Second, the homogeneous layer on top minimized the effects of evaporation and surface mixing on the linear density region.

Internal gravity waves were generated by a paddle in the upper left corner of the wave tank. The paddle had a wavelength of 24·3 cm, and consists of an oscillating piece of Plexiglas half a wavelength long, pivoted in the centre, and two pieces of thin rubber connecting the oscillating section with stationary pieces of Plexiglas. One end of the oscillating section was connected through a scotch yoke to a rotating disk, which was driven by a small motor. As the disk rotated, the Plexiglas oscillated with a frequency determined by the motor and an amplitude determined by the radial position of the connecting arm on the disk. The paddle extended across the width of the tank, and the resulting disturbances were two-dimensional.

To reduce wave reflexion from the end walls, wave absorbers were placed 2 cm from each end of the tank. The absorbers consisted of punched Plexiglas plates measuring 90·5 cm long, 28 wide and 0·6 thick. The plates were punched every 1·9 cm with holes 1·3 cm in diameter. Measurements of dye line photographs show that the wave absorbers reduced the vertical component of the amplitude of the reflected wave by a factor of almost three for the waves used in this experiment.

2.2. *Measurements and flow visualization*

Density measurements were made using double electrode conductivity probes, a Flow Research Inc. model 1104 conductivity gauge, a Dana model 4300 digital voltmeter, and strip chart recorders. The probes were constructed of stainless steel tubing with a tip made of Johnson and Johnson ADAPTIC, a commercially available dental restorative. The sensing element of the probe was thin, platinum wire, typically 0·4–0·8 mm in diameter, which was inserted through the restorative before hardening. To increase the sensitivity of the probe, the platinum wire was coated before use with a thin coating of platinum black.

A motorized traverse was used to adjust the vertical position of the probe for mean density profile measurements. Using this system, direct measurements of the mean profile could be made over a height of approximately 65 cm with an error in repeatability of well below 7 %.

Blue Dextran dye was added to the saline solution during the filling of the

tank to aid in visualizing the flow in the linearly stratified region. The dye was injected into the main solution by a small pump, which was controlled by a repeating cycle timer. This, used in conjunction with the constant flow metering pump, resulted in thin, evenly spaced, horizontal bands of coloured fluid in the linearly stratified region. During the experiment, these dye lines were lit from behind the tank with a fluorescent light source and were photographed with a 35 mm camera.

Neutrally buoyant particles were placed in the tank during some runs to visualize particle displacements. Pliolite, a Goodyear rubber compound, was used as the neutrally buoyant material. The Pliolite was first crushed, then separated into various particle sizes before being allowed to reach equilibrium levels in the tank. The neutrally buoyant particles were illuminated with vertical slits of light from both ends of the tank. The particles acted as light scattering sources for the illumination and, in a darkened laboratory, appeared as bright, point sources against a dark background. Photographs of the particles were taken with a 35 mm camera, with an exposure time of the order of one-tenth of a paddle period. Average particle velocities could be computed from these photographs, and the particle motion field was easily discernible. Examples of these photographs are shown in figure 12 (plate 3), and will be discussed in detail in §4.

3. Linear wave reflexion: theory and measurements

It is well known that, if an object is oscillated with a small amplitude in a stratified fluid with constant Brunt–Väisälä frequency, the resulting disturbances lie within bands of fluid oriented at prescribed angles to the horizontal (see e.g. Phillips 1966; Turner 1973; Mowbray & Rarity 1967; McLaren *et al.* 1973). If the frequency of oscillation is given by ω, then these angles are given by the dispersion relation for two-dimensional flow:

$$\omega = \pm N\cos\theta = \pm N\left(\frac{k_1^2}{k_1^2+k_3^2}\right)^{\frac{1}{2}},$$

provided $\omega \leqslant N$. Here N^2 is the square of the Brunt–Väisälä frequency defined by

$$N^2 = -\frac{g}{\rho}\frac{\partial\rho}{\partial z}.$$

ρ is density; z is directed vertically upward; and θ is the angle between the horizontal axis and the wavenumber $\mathbf{k}$, which has components (k_1, k_3). $k_1 = 2\pi/\lambda_x$, where λ_x is the horizontal wavelength of the forced wave and $k_3 = n\pi/H_t = 2\pi/\lambda_z$; H_t is the height of the linearly stratified region; and λ_z is the vertical wavelength of the forced wave. The particle motion is entirely transverse for this case, and the wave energy propagates along wave fronts of rays, parallel to the particle motion and at right angles to the phase velocity.

In the present experiment, waves are produced by the oscillating paddle, and the resulting disturbances are almost completely confined to bands located within rays originating at the edges of the paddle. Figure 3 shows a schematic representation of the experiment. Wave energy propagates in the direction of the rays that

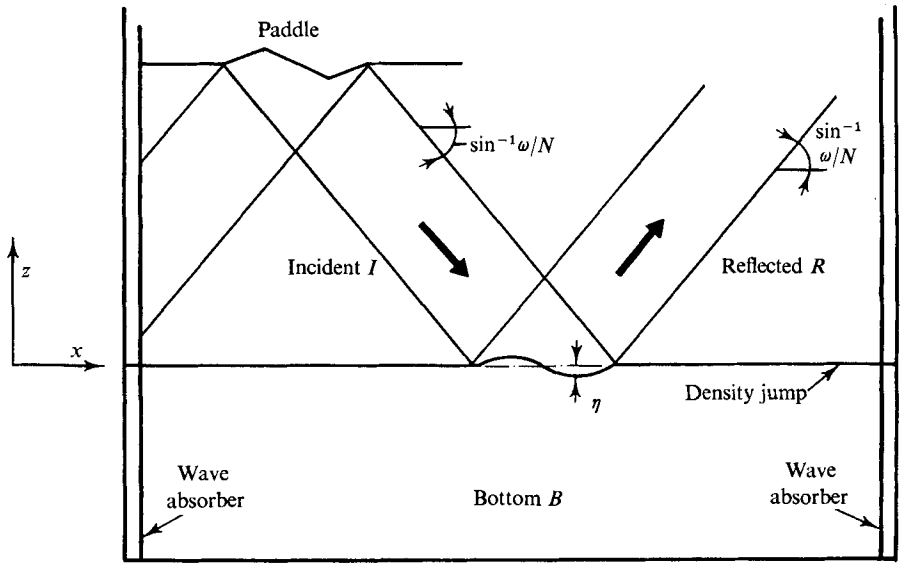

FIGURE 3. Schematic representation of the experiment. The limiting rays emanate from the edges of the paddle and are either absorbed by the side walls or reflect from the density jump. The arrows indicate the direction of the group velocity of the incident and reflected waves.

are at an angle $-\sin^{-1}\omega/N$ to the horizontal, while the phase velocity propagates normal to the rays at an angle $\pm\cos^{-1}\omega/N$ to the horizontal.

The rays propagating down and to the left of the paddle are partially attenuated by the wave absorber at the end of the tank. The rays propagating down and to the right of the paddle, however, go through the linearly stratified region, until they encounter the density jump and the constant density region below. This density profile, in which a linearly stratified layer on top is separated from a constant density layer below by a sharp density jump $\Delta\rho$ at the interface, results in a Brunt–Väisälä frequency which changes from a nearly constant value in the upper layer to zero in the constant density layer, passing through a sharp maximum in the density jump. The rays, being unable to propagate into the constant density region, reflect and propagate upward and to the right, at an angle $\sin^{-1}\omega/N$ (as shown in figure 3).

The reflexion of waves with this type of density configuration can be described by a two-layer model. We choose $z = 0$ to be the vertical position of the density jump, H_t being the height of the top layer and H_b the depth of the bottom layer. In the upper layer, where $\partial\rho/\partial z$ is constant and N is nearly so, we can assume the following forms for the vertical velocity and pressure:

$$\left.\begin{aligned} w_I &= W_I \exp i(k_1 x + k_3 z - \omega t), \quad w_R = W_R \exp i(k_1 x - k_3 z - \omega t), \\ p_I &= P_I \exp i(k_1 x + k_3 z - \omega t), \quad p_R = P_R \exp i(k_1 x - k_3 z - \omega t), \end{aligned}\right\} \tag{1}$$

for $0 \leqslant z \leqslant H_t$, where $i = \sqrt{-1}$, the subscript I denotes the incident wave, and the subscript R denotes the reflected wave. The amplitude functions W_I, W_R, P_I and P_R are complex.

In the bottom layer, N^2 is zero, and disturbances decrease exponentially with height. Letting the subscript B denote the bottom region, we assume

$$w_B = W_B \exp(k_1 z) \exp i(k_1 x - \omega t) \quad \text{and} \quad p_B = P_B \exp(k_1 z) \exp i(k_1 x - \omega t) \tag{2}$$

for $-H_b \leqslant z \leqslant 0$, where W_B and P_B are complex. The interface amplitude is defined by

$$\eta = \eta_0 \exp i(k_1 x - \omega t), \tag{3}$$

where

$$w_B = \partial\eta/\partial t.$$

Combining the continuity equation

$$\nabla . \mathbf{u} = 0$$

with the x-momentum equation

$$\rho_j \, \partial u/\partial t = -\partial p/\partial x$$

gives an equation relating the vertical velocity to the pressure:

$$\rho_j \, \partial^2 w/\partial z \partial t = \partial^2 p/\partial x^2, \tag{4}$$

which is valid in both the upper and lower layers. In the upper layer, $\rho_j = \rho_0$ to the Boussinesq approximation, and in the bottom layer $\rho_j = \rho_B$.

Since the density interface cannot sustain a pressure difference, the pressure must be continuous across the interface. To first order, this condition can be described by a balance between the dynamic pressure difference at the interface and the hydrostatic pressure, or

$$p_I + p_R - p_B = g\eta\Delta\rho \tag{5}$$

for small amplitudes η. Here $\Delta\rho$ equals the density at the top of the interface minus the density in the bottom layer. The vertical velocity must also be continuous across the interface, or

$$w_I + w_R = w_B. \tag{6}$$

Using (1) and (2) in (4), with (3), (5) and (6), gives for the reflected wave

$$W_R = \left[\frac{(\rho_0\omega^2 k_3)^2 - k_1^2(\omega^2\rho_B + gk_1\Delta\rho)^2 + i2\rho_0\omega^2 k_1 k_3(\omega^2\rho_B + gk_1\Delta\rho)}{(\rho_0\omega^2 k_3)^2 + k_1^2(\omega^2\rho_B + gk_1\Delta\rho)^2}\right] W_I, \tag{7}$$

and for the interface wave

$$W_B = \left[\frac{2(\rho_0\omega^2 k_3)^2 + i2\rho_0\omega^2 k_1 k_3(\omega^2\rho_B + gk_1\Delta\rho)}{(\rho_0\omega^2 k_3)^2 + k_1^2(\omega^2\rho_B + gk_1\Delta\rho)^2}\right] W_I, \tag{8}$$

functions of the incident wave amplitude W_I. From (7), the phase shift of the reflected wave is

$$\tan\phi = 2\left(\frac{\rho_e k_1}{\rho_0 k_3} + \beta\frac{k_1}{k_3}\right)\left[1 - \left(\frac{\rho_e k_1}{\rho_0 k_3} + \beta\frac{k_1}{k_3}\right)^2\right]^{-1}, \tag{9}$$

where we have used $\rho_B = \rho_e + \Delta\rho$ (see figure 2) and $\beta = gk_1\Delta\rho/(\rho_0\omega^2)$.

The expression β is a non-dimensional density jump, equal to the ratio of the square of the phase velocity of the interfacial wave ($C_I^2 = g\Delta\rho/(\rho_0 k_1)$) to the square of the horizontal phase velocity of the internal gravity waves

$$(C_g^2 = \omega^2/k_1^2).$$

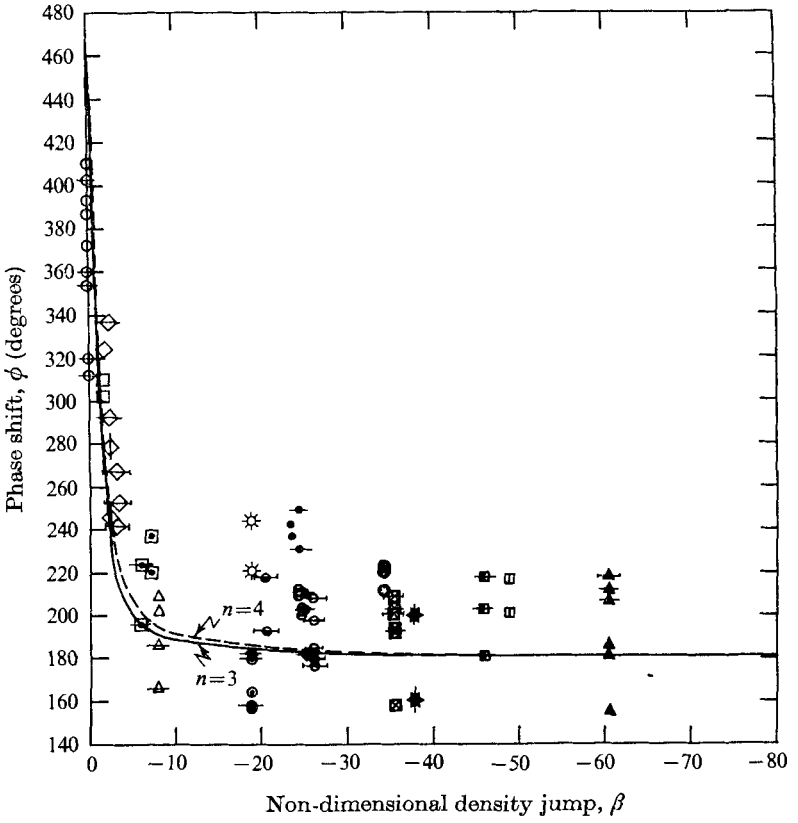

FIGURE 4. Measurements of the phase shift of the reflected wave plotted against the non-dimensional density jump β (see text). Identical symbols in figures 4 and 5 correspond to measurements made at different times during the same experimental run. The curves are from (9) for 'average' experimental conditions.

Equation (9) says that the phase shift of the reflected wave is a maximum for $\beta = 0$ ($\Delta\rho = 0$) and that $\phi = 180°$ for $\beta = -\infty$ ($\Delta\rho = -\infty$). Figure 4 shows measurements of the observed phase shift plotted against the non-dimensional density jump β. The measurements were obtained from dye line photographs taken when the observed wave amplitudes were still small. The error in the measurements is reflected by the scatter of the data points. Many different cases were run for the same value of the vertical wavenumber n, where $k_3 = n\pi/H_t$. The 'average' conditions for which data were obtained were found by averaging the parameters for all runs with the same value of n. The solid curves in figure 4 are from (9) for average experimental conditions for $n = 3$ and 4. As can be seen from figure 4, the observed phase shift rapidly approaches 180° for even small density jumps, as predicted by (9).

From (8), the non-dimensional interface amplitude is given by

$$\left|\frac{\omega\eta}{w_1}\right| = \left[1 + \left(\frac{2}{(\rho_e k_1/\rho_0 k_3) + \beta(k_1/k_3)}\right)^2\right]^{\frac{1}{2}}. \tag{10}$$

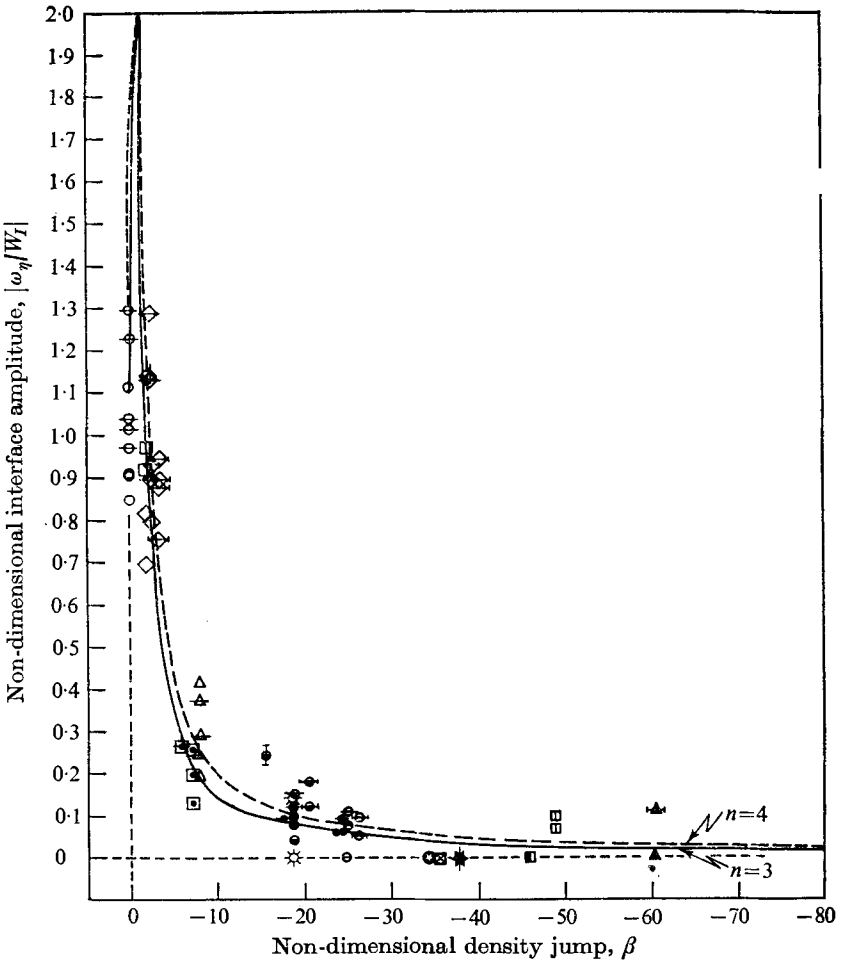

FIGURE 5. Measurements of the interface amplitude plotted against the non-dimensional density jump β. Identical symbols in figures 4 and 5 correspond to measurements made at different times during the same experimental run. The curves are from (10) for 'average' experimental conditions.

From (10), for $|\beta| \gg 1 (|\Delta\rho|$ large), $|\eta| \to 0$ and a solid wall condition is approached. The maximum interface amplitude occurs for

$$\omega^2 = -gk_1\Delta\rho/\rho_e,$$

for which $\beta \simeq -1$, and the phase velocity of the interfacial wave equals the horizontal phase velocity of the internal wave. The phase shift in this case is 360°, and the incident and reflected waves are in phase. Figure 5 shows observed values of the interface amplitude and curves of (10) for different values of n. The measurements are taken from dye line photographs of the experiment; they show that the observed interface amplitude is large only for small values of β. Figure 5 shows that, when $\beta \simeq -1$, the observed values of the interface amplitude are less than the values predicted from (10). This may be due to the uncertainty of measuring β for small values of $\Delta\rho$, or to the difficulty of setting up experimentally the conditions for which $\beta \simeq -1$.

When $|\beta| \sim \sigma(1)$ ($|\Delta\rho|$ small), the maximum amplitude occurs at the interface while when $|\beta| \gg 1$ ($|\Delta\rho|$ large), the maximum amplitude occurs in the region where the incident and reflected waves interact. This shift in the location of maximum amplitude is because of the phase shift of the reflected wave. Figure 6 (plate 1) is two photographs of the wave tank under the same conditions, except for different density jumps. Both photographs show the wave paddle in the upper left corner of the tank, and the wave motion extending away from the paddle as shown in figure 3. Limiting rays have been sketched in figure 6 (*a*), to show the incident and reflected wave regions. Arrows have also been drawn in to show the direction of the incident and reflected group velocities. Dye lines are shown in the photographs as white and in the linearly stratified region. The lowest dye line indicates the bottom of the linearly stratified region and the beginning of the density jump. In figure 6 (*a*), the density jump is very small, and the maximum amplitude occurs near the interface. In figure 6 (*b*), the density jump is much larger, and the maximum amplitude occurs in the interaction region with the interface remaining virtually flat. The change in phase shift of the reflected wave can be seen by comparing figure 6 (*a*) with figure 6 (*b*).

From (7) the ratio of the amplitudes of the reflected wave to the incident wave can be shown to be

$$|W_R/W_I| = 1, \tag{11}$$

for all values of the density jump $\Delta\rho$. Thus, the amplitude of the vertical velocity of the reflected wave is equal to the amplitude of the vertical velocity of the incident wave for all values of the density jump. A similar result was found by McKenzie (1972), who solved for the reflexion coefficient of acoustic–gravity waves at an interface separating two layers of constant, but unequal, density. This means that, in the steady state, the energy in the incident wave E_{I}, which equals the outgoing energy E_{O}, must vary with $\Delta\rho$, such that the total energy $E_{\mathrm{I}}+E_{\mathrm{O}}+E_A = 2E_{\mathrm{I}}+E_A$ remains constant (E_A is the absorbed energy). Thus, for equal paddle amplitudes, the incident wave amplitude should be larger for a large density jump than for a small density jump. This effect is expected to be small; and no differences in wave amplitude could be observed from the data.

Equation (11) can be justified by deriving the energy fluxes in the top and bottom regions. We choose a control volume such that the bottom surface is far enough away from the density jump that disturbances are negligible there. The energy equation

$$DE/Dt = -\nabla . p\mathbf{u}$$

is averaged over x in the top region and integrated from $z = 0$ to $z = z_t$. Assuming periodicity in x, this gives

$$\int_{z=0}^{z_t} \overline{DE/Dt}^x \, dz = -(\overline{p_t w_t^x})_{z=z_t} + (\overline{p_t w_t^x})_{z=0}.$$

The subscript t indicates the top region. In the bottom region, when we average over x and integrate the kinetic energy from $z = z_b$ to $z = 0$, we get

$$\int_{z=z_b}^{0} \overline{DK/Dt}^x \, dz = -(\overline{p_b w_b^x})_{z=0}.$$

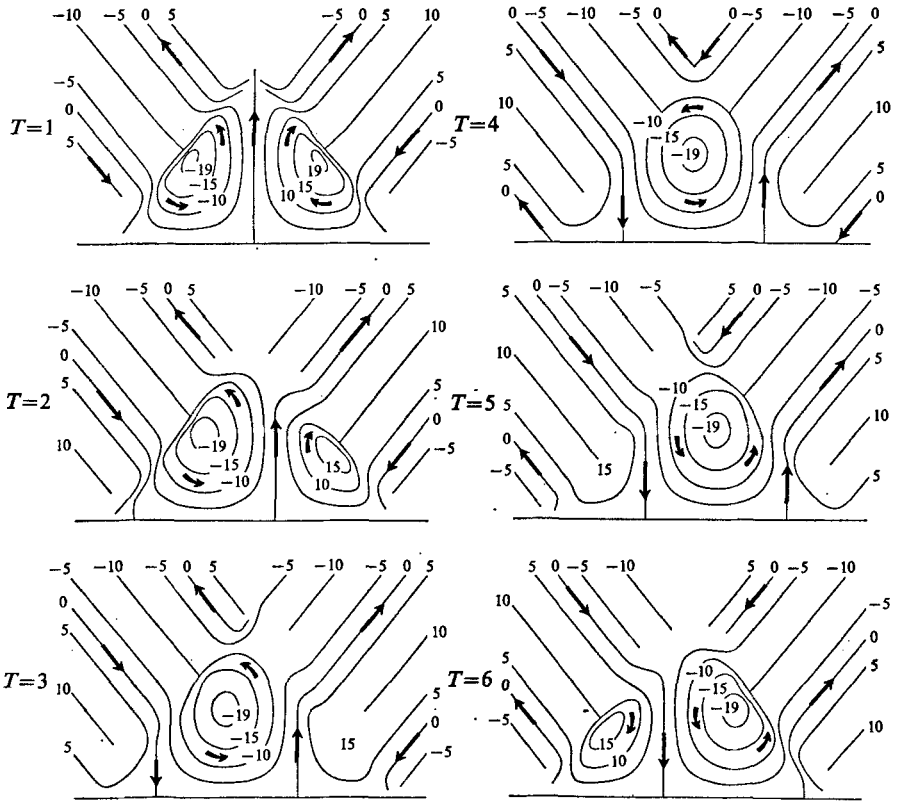

FIGURE 7. Stream function contours plotted every second for half a wave period in the region where the incident and reflected waves interact (refer to figure 3). The horizontal line at the bottom of each plot represents the density jump with $\eta = 0$. The interaction region is most easily seen in the first plot ($T = 1$), which shows the incident wave region on the left, the interaction triangle and the reflected region on the right. The contour labels are in arbitrary units. The arrows indicate the directions of particle motion.

The subscript b indicates the bottom. Now, p_b is connected to p_t at $z = 0$ through the boundary condition (5). Also, since $w\eta = \frac{1}{2}\eta^2)_t$ and $-g\Delta\rho\,(\frac{1}{2}\eta^2)_t$ is the time derivative of the potential energy of the interface, we get for the bottom layer

$$\int_{z=z_b}^{0} \overline{DE/Dt}^x\,dz = -\overline{(p_t w_t^x)}_{z=0}.$$

Thus,

$$\int_{z=z_b}^{z_t} \overline{DE/Dt}^x\,dz = -\overline{(p_t w_t^x)}_{z=z_t},$$

or, for steady-state conditions,

$$\overline{p_t w_t^x} = 0 \quad \text{at} \quad z = z_t. \tag{12}$$

Thus, from (12) an incident wave must be balanced by a reflected wave of equal strength passing through the top surface of the control volume, and (11) follows.

The reflexion of energy from the density jump causes a complicated flow pattern to appear in the interaction region. Streamlines for this region are shown in

Experiment ...	(i)	(ii)	(iii)	(iv)	(v)	(vi)	(vii)	(viii)
$\Delta\rho$ ...	−0·021	−0·021	−0·052	−0·052	−0·028	−0·028	−0·009	−0·008
H_t ...	41	41	42	42	47	47	44	50
T_{BV} ...	8·17	7·52	7·88	7·88	8·06	8·50	8·05	8·55
Run								
1	10·6	10·2	10·7	12·0	10·0	12·4	10·5	10·5
2	10·6	11·8	10·6	12·0	9·2	12·9	10·5	10·4
3	8·7	12·0	12·0	—	11·7	13·0	10·5	9·5
4	9·6	11·6	12·0	—	13·5	12·9	12·0	9·5
5	9·8	11·8	10·6	—	11·4	—	—	9·7
6	9·5	10·3	9·2	—	11·9	—	—	—
7	11·0	8·8	9·3	—	11·9	—	—	—
8	14·9	—	9·2	—	—	—	—	—
9	—	—	8·2	—	—	—	—	—

Experiment ...	(ix)	(x)	(xi)	(xii)	(xiii)	(xiv)	(xv)	(xvi)
$\Delta\rho$ ...	−0·026	−0·022	−0·025	−0·049	−0·050	−0·052	0	−0·002
H_t ...	44	44	44	44	44	44	46	43
T_{BV} ...	8·07	7·81	8·69	8·20	8·35	8·62	8·65	8·20
Run								
1	10·8	8·8	11·3	9·3	10·9	11·2	9·8	10·8
2	10·8	10·2	—	10·8	—	—	11·0	—
3	10·5	10·2	—	—	—	—	—	—
4	10·5	—	—	—	—	—	—	—
5	10·3	—	—	—	—	—	—	—
6	10·5	—	—	—	—	—	—	—
7	10·5	—	—	—	—	—	—	—

Experiment ...	(xvii)	(xviii)	(xix)	(xx)	(xxi)	(xxii)	(xxiii)	(xxiv)
$\Delta\rho$ ...	−0·002	−0·002	−0·002	−0·025	−0·026	−0·028	−0·028	−0·034
H_t ...	43	45	45	43	43	43	43	43
T_{BV} ...	8·47	8·35	8·35	8·45	8·58	8·57	8·57	8·71
Run								
1	9·8	10·0	10·3	11·1	11·2	11·5	11·5	11·4
2	11·2	10·0	10·6	11·2	11·2	11·6	11·5	11·4
3	13·0	10·1	10·7	11·3	11·4	11·5	—	11·4
4	11·2	10·4	11·0	11·4	11·7	—	—	—
5	—	10·8	11·2	—	11·7	—	—	—
6	—	—	11·4	—	—	—	—	—
7	—	—	11·7	—	—	—	—	—
8	—	—	11·9	—	—	—	—	—
9	—	—	11·0	—	—	—	—	—

Experiment ...	(xxv)	(xxvi)	(xxvii)
$\Delta\rho$ ...	−0·034	−0·034	−0·034
H_t ...	43	43	43
T_{BV} ...	8·77	8·75	8·75
Run			
1	11·4	11·4	11·4
2	11·4	11·4	—
3	11·4	11·4	—
4	—	11·4	—

TABLE 1. For each experiment, summary of the paddle period $T_p(i, \text{run})$, and the density jump $\Delta\rho$ (g cm^{-3}), the height of the linearly stratified region H_t (cm), and the Brunt–Väisälä period of the linearly stratified region $T_{BV}(i)$

figure 7 for half a wave period. These patterns were obtained numerically by the linear superposition of two waves, assuming a phase shift of 180°. The streamlines have been smoothed near the edges of the interaction triangle, since in the model disturbances fall discontinuously to zero outside the limiting rays. The moving eddy pattern shownin figure 7 has been observed from streakline photographs of the interaction region. Measurements from these streakline photographs and dye line photographs for small amplitude waves show that the horizontal velocities and amplitudes in the interaction region are approximately twice that of the incident wave, as predicted by linear theory.

Table 1 provides a summary of the experiments performed, and lists the Brunt–Väisälä period T_{BV}, the paddle period T_p, the measured value of the density jump $\Delta\rho$, and the height of the linearly stratified region H_t, for all of the experiments and for each run within an experiment.

4. Breaking of internal gravity waves

As discussed earlier, the wave amplitude is a maximum close to the interface in the region where the incident and reflected waves interact. When this amplitude becomes large enough, a local gravitational instability appears in the flow in the form of an S shape in the dye lines, and the wave is said to overturn or break. Figure 8 (plate 2) is a photograph of the wave tank with large $\Delta\rho$, taken at a time when overturning was present in the interaction region. Arrows have been added to the figure to indicate the direction of the group velocities of the incident and reflected waves; and a rectangle has been superimposed around the dye lines in the interaction region. The characteristic S shape of an overturning dye line can be seen inside the rectangle. The S shape indicates that heavy fluid from below the dye line is now overlying lighter fluid from above the dye line, and that the region is gravitationally unstable.

The stages in the overturning process are displayed in figure 9, which shows traces from an 8 mm movie film of the dye lines in the interaction region during overturning. The vertical scale of the traces is exaggerated for clarity. Overturning begins when $\partial\rho/\partial z$ is locally unstable, as shown in the first trace. The wave, as visualized by the dye line, propagates to the right, but the overturned region remains practically stationary. The trough of the wave thus catches up with the overturned region, and the second trace shows the overturning apparently in the trough of the wave. The overturned region collapses vertically and spreads horizontally owing to the unstable density gradient, as each particle seeks a neutral level in the stratified region. The collapse and spreading of the unstable region results in areas of large, local density gradients. These gradients would appear as sharp lines on a shadowgraph, and are possibly the 'traumata' mentioned by McEwan (1971, 1973) in his experiments. The overturning and collapse of the unstable region also results in local patches of turbulence which help smooth out the large gradients formed by the collapsing region. The spreading and smoothing of the unstable region continues as the region is lifted vertically by the crest of the next wave. By the time this crest reaches the location where the overturning began, no visible traces are left of the previous instability, as

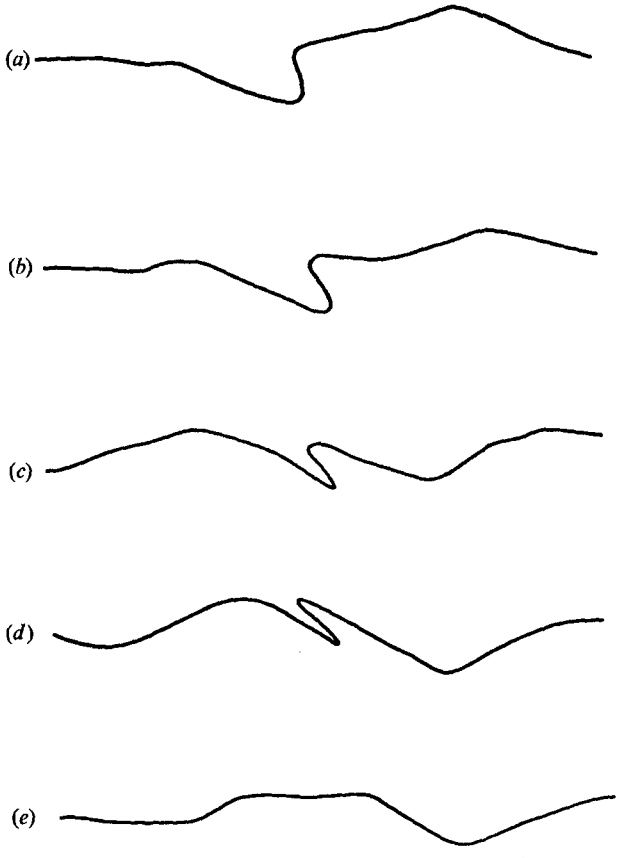

FIGURE 9. Series of dye line traces taken from an 8 mm movie film at equal time intervals during an overturning sequence. The vertical scale has been exaggerated for clarity.

shown by the last trace. Throughout the overturning process, the breaking region and the local turbulence produced by the overturning appear to be stationary in the laboratory frame, and do not propagate horizontally with the wave. The overturning occurs along lines that lie at an angle to the horizontal, which is less than the angle the rays make to the horizontal (as can be seen from figure 8, plate 2). In the present study, it is found experimentally that this 'line of breaking' angle is approximately one-half the angle the rays make to the horizontal, although it is not obvious that this result need be true generally. Smaller wavelength waves appear prior to overturning as small perturbations on the dye lines in the interaction region. Once breaking occurs, however, the amplitudes of these higher wavenumbers appear to grow as a result of the overturning. These higher wavenumbers can be seen in both the dye line photograph of figure 8 and in the traces of figure 9.

The observed horizontal wavelengths λ_x of the waves generated by the paddle were approximately 18–21 cm, and slightly smaller than the paddle itself. This wavelength appeared to vary according to the angle the rays made to the horizontal and to the paddle amplitude; but it was difficult to make exact measurements because of uncertainties in obtaining the wavelength from the dye line

photographs. These changes in horizontal wavelength were apparently caused by the paddle itself, and by the design of the wave generator.

With $|\Delta\rho|$ large, the largest wave amplitudes were believed to occur when the paddle was oscillated with a frequency corresponding to one of the resonant frequencies of the linearly stratified region, i.e.

$$\omega^2 = N^2 k_1^2/(k_1^2 + k_3^2),$$

$k_3 = n\pi/H_t$; n is an integer. Measurements of λ_x, H_t and the angle between the rays and the horizontal $\tan^{-1}\lambda_z/\lambda_x$ indicate that, to within experimental error, for the cases when the waves broke, n was an integer. These measurements were confirmed by measuring the vertical wavelength λ_z from the dye line photographs. When $\Delta\rho$ is zero, n is probably a half-integer, to allow the maximum amplitude to occur at the interface. Experimental verification for these cases is inconclusive because of the larger errors involved in measuring λ_z when $|\Delta\rho|$ is small. Although the resonant frequencies were believed to produce the largest wave amplitudes, no true resonance was observed, since the observed wave amplitudes were always of the same order of magnitude as the paddle amplitude.

Figure 10 shows the amplitudes of many waves just prior to overturning or, in the cases where no breaking was observed, the maximum observed amplitude of the wave. In the cases with large $\Delta\rho$ for which breaking occurred, different symbols are used for the different values of n. For the cases where breaking did not occur, slightly different symbols from the breaking symbols are used; and, for these cases, the value of n is close to the integer shown. In two cases of breaking, the value of n was uncertain, and these cases are marked by different symbols. No values of n are given when $\Delta\rho$ is small, owing to the uncertainty in λ_z referred to above.

The amplitudes shown in figure 10 were measured from dye line photographs just prior to breaking or at the end of our experimental run. The errors in reading the dye line amplitudes from these photographs is estimated at around 30%. Conductivity probe traces were also made during some of these runs; but these traces had insufficient frequency response (because of the lack of washout at the probe tip) to deduce wave amplitude. An oscillating conductivity probe system is currently being tested, and has had encouraging preliminary success in overcoming these difficulties. Details on this system will be given elsewhere.

From figure 10, it is seen that there appears to be a critical amplitude above which overturning will occur, and below which it will not; Orlanski (1972), in his study of standing internal gravity waves, showed that the theoretical critical amplitude of an isopycnic line is given from linear theory by

$$(\Delta z)_{\max} \simeq 0{\cdot}739 H_t/(n\pi). \tag{13}$$

Values of $(\Delta z)_{\max}$ from (13) for $n = 3$ and 4 are shown in figure 10, to give an idea of where the theoretical critical amplitudes lie for the runs shown in the present experiment. The data for breaking waves in this experiment are best fitted by the curve

$$(\Delta z)_{\exp} \simeq 0{\cdot}44\, H_t/(n\pi).$$

The discrepancy between this curve and the theoretical curve (13) may be due

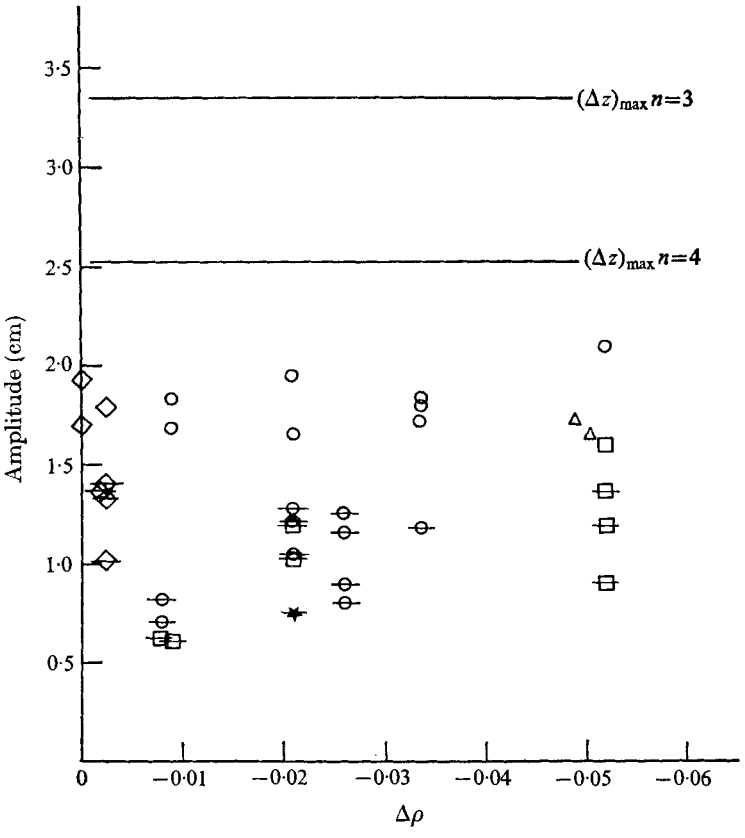

FIGURE 10. Measured wave amplitude (cm) as a function of $\Delta\rho$ (g cm^{-3}). The values of $(\Delta z)_{max}$ are from (13). ○, $n = 3$, breaking; ⊖, $n = 3$, no breaking; ⊟, $n = 4$, breaking; □, $n = 4$, no breaking; ★, $n = 5$, no breaking; △, $n = 3$ or 4, breaking; ◇, $\Delta\rho$ small, breaking; ◈, $\Delta\rho$ small, no breaking observed.

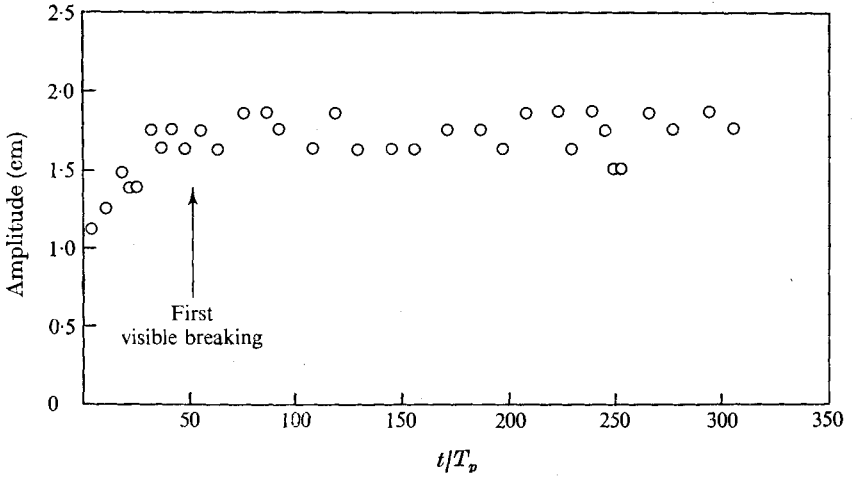

FIGURE 11. Measured wave amplitude as a function of wave periods after the paddle was started.

to the large errors involved in reading the small amplitudes in the dye line photographs, nonlinear effects not treated in (13), and impurities in the forcing function introduced by the wave paddle.

Figure 11 shows a typical plot of wave amplitude as a function of time, expressed as wave periods after the paddle was started, and shows that breaking limits the maximum amplitude of the wave. Similar results were shown by Orlanski (1972) for the standing wave experiment. Comparing this with the case of an unstable Kelvin–Helmholtz wave, Delisi (1972) and Delisi & Corcos (1973) have shown that waves, which grew as the result of shear instability, continued growing after the onset of overturning. In their experiments in a stratified-flow wind tunnel, the maximum potential energy of an unstable Kelvin–Helmholtz wave occurred after the wave had started overturning; thus, the overturning did not necessarily halt the growth of the wave. In the present experiment, overturning limited the growth of the wave, and the maximum amplitude the wave attained occurred just prior to overturning.

Streak photographs of neutrally buoyant particles were taken in some experiments, to gain additional information on fluid motion and particle velocities. Figure 12 (plate 3) is three of these streak photographs taken at different times during a run at the same phase angle of the wave in the interaction region. Two conductivity probes are shown in the photographs, and dye lines appear as faint dark bands. The dye line just below the streaks indicates the bottom of the linearly stratified region and the beginning of the density jump.

Figure 12 (*a*) shows a streak photograph of the interaction region taken before the onset of breaking. The eddy shown in the streamline plots of figure 7 can be seen just to the right of the probes. The sense of the eddy can be deduced from the dye lines, and, in this case, particle motion is counter-clockwise. The arrows in the fourth plot of figure 7 show the directions of particle motion in these photographs. The particle motions shown follow fairly well those computed numerically from the linear superposition of two waves integrated over the exposure time of the photograph. Based on the computed particle motions, it can be shown that the average particle velocities read from the streak photographs can be in error from the maximum particle velocity by as much as 40–50 %, particularly at the top of the interaction region. This large reading error is caused both by the long exposure time of the streak photograph, and by the fact that the maximum velocity appears in the top of the interaction region only very briefly.

The regular, ordered particle structure shown in figure 12 (*a*) is repeated with little observable change from period to period while the wave amplitude is small. As the amplitude of the wave increases, a horizontal advection of density takes place, as shown by the streak photograph in figure 12 (*b*), which was taken near the onset of breaking. In this figure, the axis of the eddy has shifted counter-clockwise from the vertical, and a kink in the particle motions can be seen along the upper left edge and the lower right edge of the eddy where regular, smooth patterns had been observed before. In this stage in the development of the wave, small changes in the flow field can be observed from one period to the next.

The distortion of the wave field caused by the advection of density evident in figure 12 (*b*) eventually causes local unstable density gradients to form. This is

apparent in the streak photograph of figure 12(*c*), which was taken during overturning. Orlanski & Bryan (1969) have shown that, for local unstable density gradients to appear, the horizontal advection of density must balance the local time rate of change of density. This is true for a single wave when the horizontal velocity u equals or exceeds the horizontal phase velocity. Thus, in the present experiment

$$u \geqslant \lambda_x/T_p \sim 1{\cdot}5\,\mathrm{cm\,s^{-1}}.$$

Average velocities of the order of 1 cm s^{-1} can be read from the streak photographs, and even larger velocities appear to be present at the bottom of the eddy. Thus, with an estimated error of 50 % between the measured, average velocities and the maximum velocity, the results are consistent with the overturning mechanism of Orlanski & Bryan. In figure 12(*c*), the eddy is greatly distorted, and the large horizontal advection of density at the top of the interaction region has caused an unstable density gradient to form just above the base of the conductivity probes. Smaller-scale motions are now evident in this photograph, and the distortion of the wave field has caused the original eddy to split into two smaller eddies. The unstable density gradient and the splitting of the eddy shown in this photograph lie along a line oriented at approximately half the angle that the rays make to the horizontal; it is the same 'line of overturning' discussed in reference to figure 8. The characteristic height of overturning measured from the streak photographs is approximately 2 cm. Overturning has a catastrophic effect on the wave field, and the repeatability and regularity of the flow field before the onset of breaking has now been replaced by a large variance and lack of repeatability from one wave period to the next.

Observationally, overturning causes a decrease in the amplitude of the reflected wave. The decreased amplitude must be a measure of the energy transferred from the incident wave to the turbulence produced by overturning. No attempt was made to measure this transfer of energy, from the data.

Before several experimental runs, a detailed vertical density profile was made of the interaction region and the density jump with a conductivity probe and a micrometer traversing mechanism capable of reading the vertical position of the probe tip to within $\pm 0{\cdot}005$ cm. The paddle was then started, and violent overturning was allowed to occur for up to one and a half hours. A second detailed density traverse was then made, in an attempt to discover the effects of the overturning and the resulting turbulence on the original density profile, either in the form of a step in density or as a sharpening of the top of the density jump. To within experimental accuracy, no differences in the two density profiles were ever observed. It was postulated that no difference was seen in the profiles because the overturning and turbulence occurred in localized regions of the wave tank. Thus, any localized distortion of the mean density profile would be difficult to detect when spread out over the entire horizontal area of the wave tank.

5. Conclusions

A laboratory experiment has been presented which examined the role of density jumps in the reflexion and overturning of internal gravity waves. The main conclusions of the study are the following. (i) The measured phase shift of the reflected wave and the measured amplitude of the density jump are in good agreement with linear theory. (ii) When the wave amplitude becomes large in the region of interaction, local overturning occurs. (iii) There appears to be a critical amplitude above which local overturning will occur and below which it will not. For the data presented here, the observed critical amplitude is

$$\Delta z \simeq 0{\cdot}44 H_t/(n\pi).$$

(iv) The overturning appears to be due to local gravitational instability, caused by the horizontal advection of density. (v) Streak photographs using neutrally buoyant particles show that overturning changes the basic flow field in the region of interaction. Smaller-scale motions can be observed in this region as a result of the overturning.

The authors would like to express appreciation to their co-workers at the Geophysical Fluid Dynamics Laboratory for their support and encouragement throughout this study, in particular to Dr B. B. Ross for many stimulating discussions and for help in clarifying the manuscript. Our thanks also to Mr M. Candelori for aid in constructing the experimental apparatus, to Mr J. N. Conner for photographic assistance, to Mr P. G. Tunison for drafting the figures, and to Mrs B. M. Williams for typing the manuscript. In addition, one of the authors (D. P. D.) would like to express his appreciation to the National Research Council for the support of an NRC/NOAA Resident Research Associateship. This research was part supported by NSF grant GA-14955 to Princeton University.

REFERENCES

Delisi, D. P. 1972 An experimental study of finite amplitude waves in a stratified wind tunnel. Ph.D. thesis, Department of Mechanical Engineering, University of California at Berkeley.

Delisi, D. P. & Corcos, G. 1973 A study of internal waves in a wind tunnel. *Boundary-Layer Meteorol.* **5**, 121–137.

Fortuin, J. M. H. 1960 Theory and application of two supplementary methods of constructing density gradient columns. *J. Polymer Sci.* **44**, 505–515.

Gossard, E. E., Richter, J. H. & Jensen, D. R. 1973 Effect of wind shear on atmospheric wave instabilities revealed by FM/CW radar observations. *Boundary-Layer Meterol.* **4**, 113–131.

McEwan, A. D. 1971 Degeneration of resonantly-excited standing internal gravity waves. *J. Fluid Mech.* **50**, 431–448.

McEwan, A. D. 1973 Interactions between internal gravity waves and their traumatic effect on a continuous stratification. *Boundary-Layer Meterol.* **5**, 159–175.

McKenzie, J. F. 1972 Reflection and amplification of acoustic-gravity waves at a density and velocity discontinuity. *J. Geophys. Res.* **77**, 2915–2926.

McLaren, T. I., Pierce, A. D., Fohl, T. & Murphy, B. L. 1973 An investigation of internal gravity waves generated by a buoyantly rising fluid in a stratified medium. *J. Fluid Mech.* **57**, 229–240.

Mowbray, D. E. & Rarity, B. S. H. 1967 A theoretical and experimental investigation of the phase configuration of internal waves of small amplitude in a density stratified liquid. *J. Fluid Mech.* **28**, 1–16.

Orlanski, I. 1972 On the breaking of standing internal gravity waves. *J. Fluid Mech.* **54**, 577–598.

Orlanski, I. & Bryan, K. 1969 Formation of the thermocline step structure by large-amplitude internal gravity waves. *J. Geophys. Res.* **74**, 6975–6983.

Pao, Y. & Goldberg, A. (eds.) 1969 *Clear Air Turbulence and Its Detection.* New York: Plenum Press.

Phillips, O. M. 1966 *The Dynamics of the Upper Ocean.* Cambridge University Press.

Scotti, R. S. & Corcos, G. M. 1972 An experiment on the stability of small disturbances in a stratified free shear layer. *J. Fluid Mech.* **52**, 499–528.

Thorpe, S. A. 1968 A method of producing a shear flow in a stratified fluid. *J. Fluid Mech.* **32**, 693–704.

Thorpe, S. A. 1969 Experiments on the instability of stratified shear flows: immiscible fluids. *J. Fluid Mech.* **39**, 25–48.

Thorpe, S. A. 1971 Experiments on the instability of stratified shear flows: miscible fluids. *J. Fluid Mech.* **46**, 299–319.

Thorpe, S. A. 1973 Turbulence in stably stratified fluids: a review of laboratory experiments. *Boundary-Layer Meterol.* **5**, 95–119.

Turner, J. S. 1973 *Buoyancy Effects in Fluids.* Cambridge University Press.

Woods, J. D. & Wiley, R. L. 1972 Billow turbulence and ocean microstructure. *Deep-Sea Res.* **19**, 87–121.

(*a*)

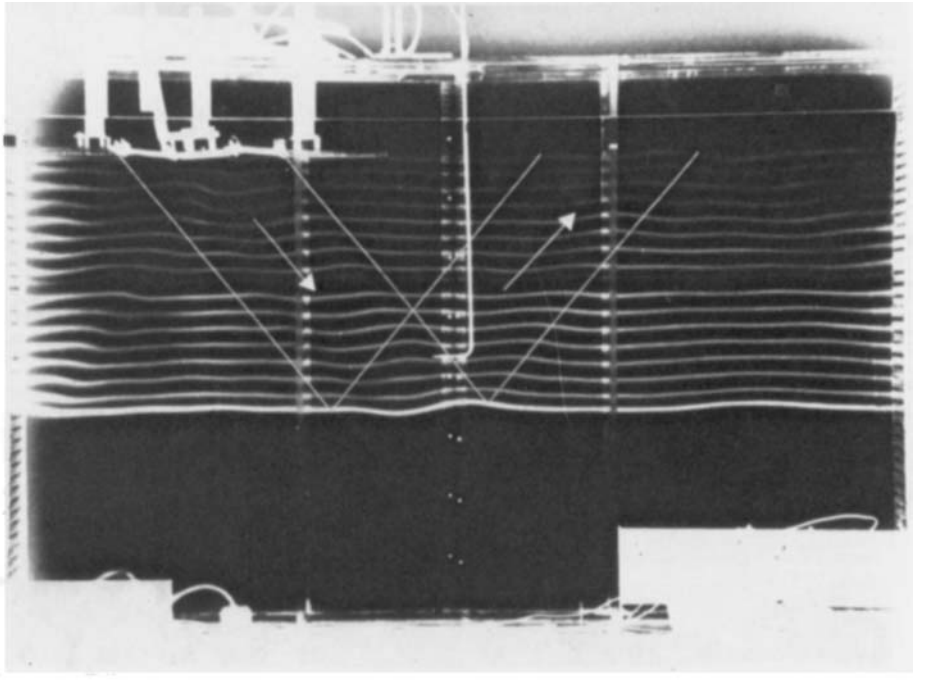

(*b*)

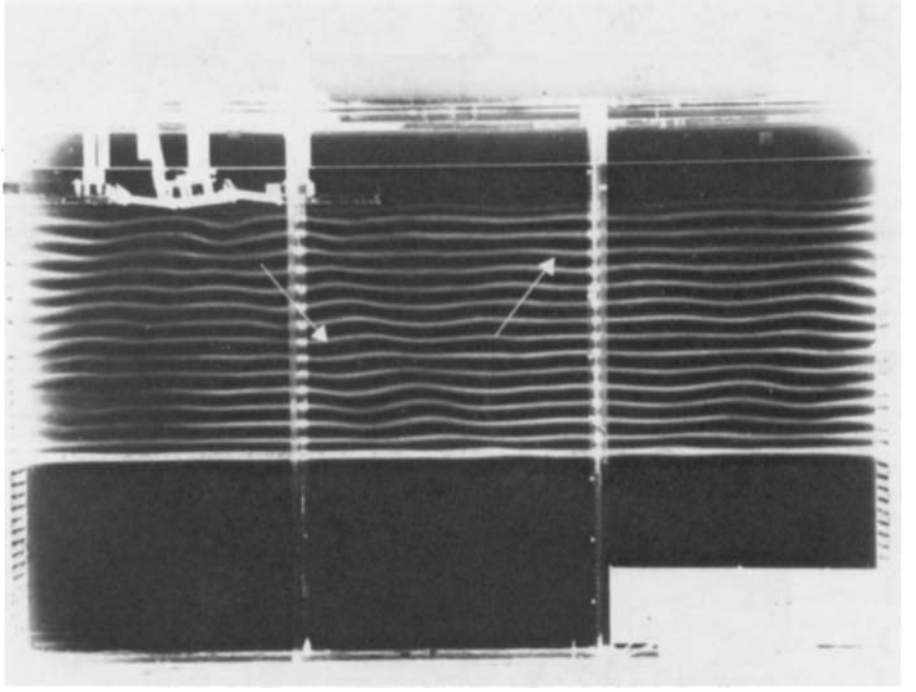

FIGURE 6. For legend see next plate.

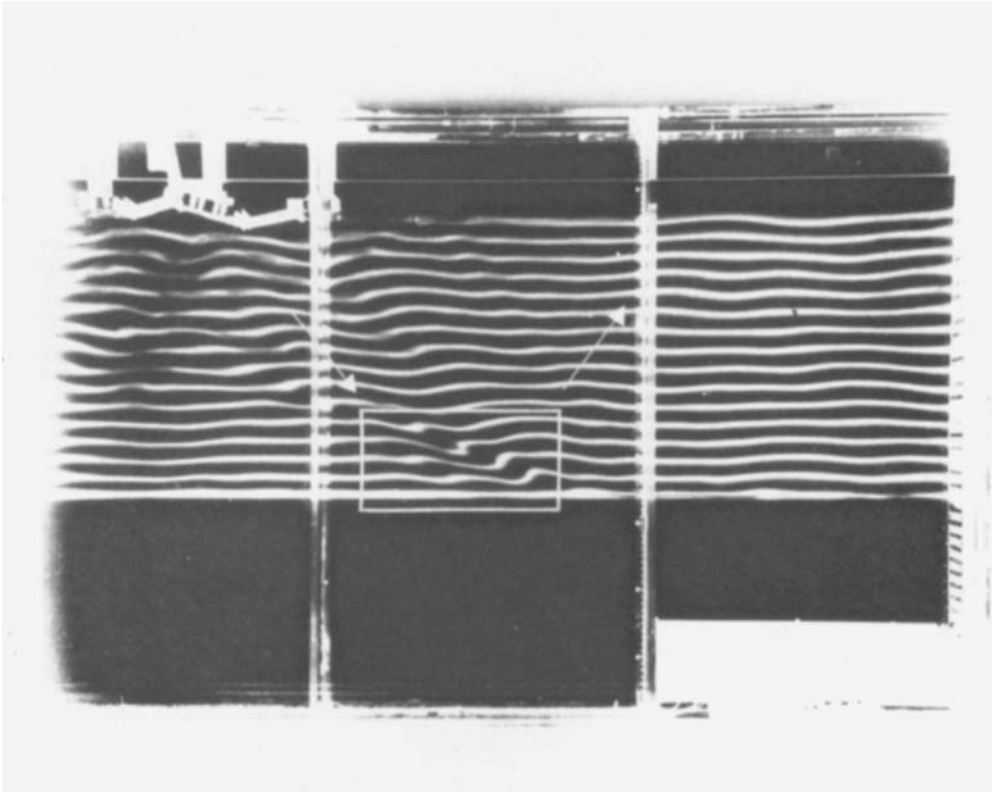

FIGURE 8. Photograph of the wave tank during overturning in the interaction region. The characteristic S shape of an overturning dye line can be seen inside the white box that outlines the region of interest. The arrows indicate the direction of the incident and reflected group velocity. The photograph was taken during experiment (xxvi), run 1.

Legend to FIGURE 6.

FIGURE 6. Photographs of the wave tank during two experimental runs. In both photographs the wave paddle is located in the upper left corner of the tank, and dye lines appear in the linearly stratified region as white, horizontal lines. The lowest dye line indicates the bottom of the linearly stratified region and the top of the density jump. The wave absorbers can be seen near the end walls of the tank, and the outline of a clock is shown in the lower right corner. The arrows indicate the directions of the group velocity of the incident and reflected waves. (*a*) Experiment (xvi), run 1. The density jump is small ($\beta = -1{\cdot}9$), and the maximum amplitude occurs near the interface. (*b*) Experiment (xxvii), run 1. The density jump is much larger ($\beta = -35{\cdot}5$), and the interface remains virtually flat. The maximum amplitude now occurs in the interaction region.

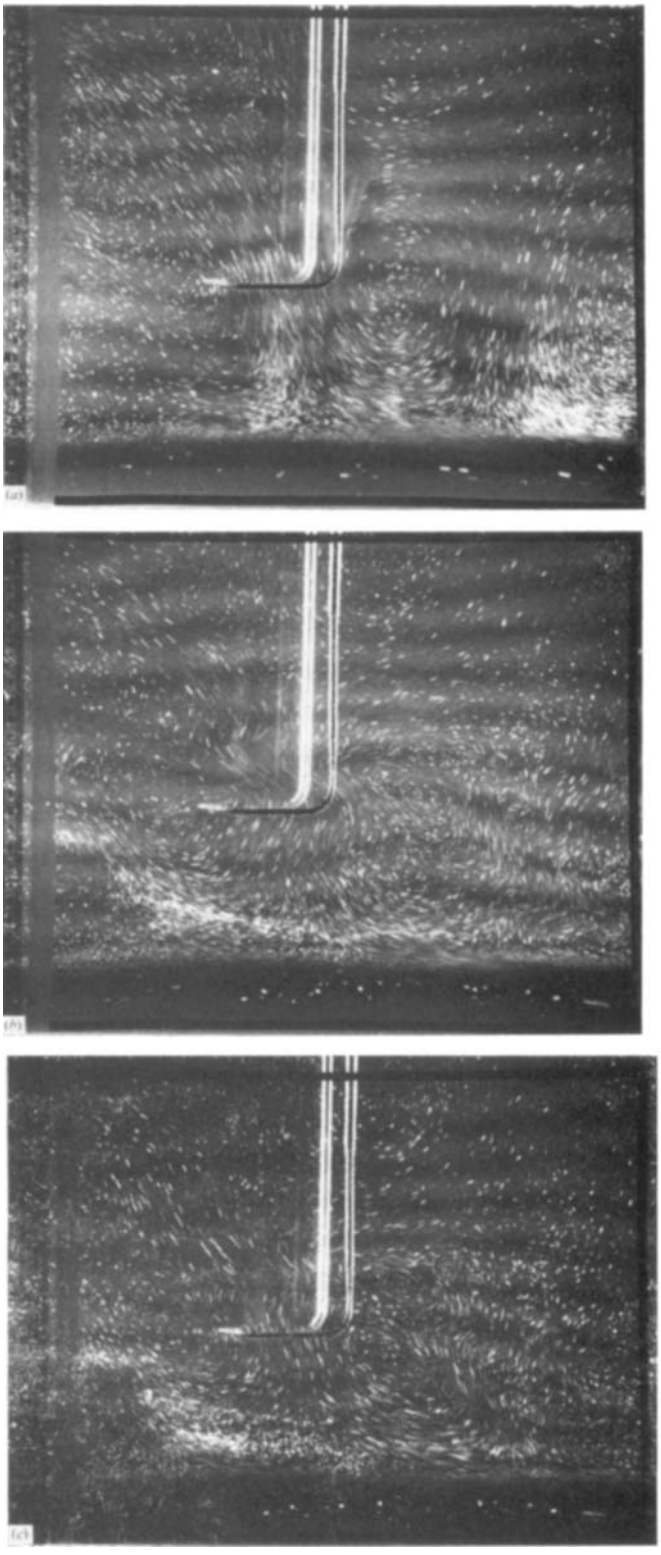

FIGURE 12. Series of three streak photographs of the interaction region taken at different times during an experimental run. Two conductivity probes are shown in each photograph, and the scale at the left is marked in cm. (*a*) Before the onset of overturning, (*b*) near the onset of overturning, and (*c*) during overturning.